Ultrafast Quantum Control in Atoms and Molecules

Philip H. Bucksbaum

Physics Department, University of Michigan
Ann Arbor, MI 48109-1120

Abstract. This paper reviews recent progress in experiments to control quantum dynamics in condensed phase and gas phase systems, using shaped ultrafast radiation. Many of the same techniques that have led to laser pulses in the 10 *fs* - 100 *ps* range can also be applied to the control of quantum systems with similar dynamical time scales. Systems under study include electron wave packets in Rydberg atoms, chemical dynamics in molecular liquids and lattice dynamics in crystalline solids. The feature common to each of these systems is ultrafast response. Shaped intense ultrafast radiation initiates the dynamics, which can then be studied using several new techniques.

INTRODUCTION

Quantum control aims to go beyond observations of atomic and molecular properties, to manipulate the dynamics of quantum systems using strong external fields. This paper summarizes recent techniques for controlling motion on the quantum scale, and also describes some recent applications in this new field. One of our goals has been the construction of a "learning machine," that is, an automated experimental apparatus that can use feedback signals from a quantum system to help optimize control strategies for a particular application. The learning machine consists of a learning algorithm, together with programmable experimental inputs and readouts. Learning machines could be particularly useful for controlling systems where the Hamiltonian is not known completely.

On a different level, wave packets are forms of information stored in the quantum system. We have studied some simple examples where information is stored as quantum phase in a Rydberg wave packet, and then efficiently extracted by converting the phase information to quantum amplitudes.

This paper will describe some basic aspects wave packet shaping and control, and then summarize our work on learning algorithms and quantum information storage.

CP551, *Atomic Physics 17,* edited by E. Arimondo, P. DeNatale, and M. Inguscio

SHAPING ULTRAFAST OPTICAL PULSES

Our optical pulses are formed in a Kerr-Lens mode-locked titanium sapphire oscillator[1]. Such lasers are capable of producing hundreds of nanometers of coherent bandwidth, although we typically only use about 10 nm. The output is amplified in a 10 Hz regenerative chirped-pulsed amplifier[2]. The output pulse is approximately 100 fsec long, with a central wavelength of about 790 nm.

Ultrafast laser pulses contain approximately two to 50 optical cycles, and last only a few femtoseconds. This is much faster than any current electronics and therefore shaping with fast time gates is very difficult. On the other hand, optical pulse bandwidths range from several tens of percent to only a few percent of the optical spectrum. Such large bandwidths are relatively easy to measure and to filter, and there are several techniques to shape the spectrum, and thereby shape the temporal pulse. In our pulse shaper, individual frequency components in the pulse are controlled by passing the light through two back-to-back spectrometers, which are configured to introduce zero net temporal dispersion: that is, all colors pass through the spectrometers in the same amount of time. The first spectrometer spreads the unshaped pulse spectrum along a line in the image plane, where the light intercepts a spatial amplitude and phase mask. The mask output then forms the entrance to a second spectrometer, which recombines the colors into a single shaped pulse.

The heart of the pulse shaper is the programmable mask that forms the Fourier filter. This mask must be capable of either attenuating the individual colors or shifting their phase. Two different electronically programmable masks that are capable of controlling both amplitude and phase have been demonstrated: a liquid crystal display (LCD) and an acousto-optic modulator (AOM).

We use an AOM design originally developed at Princeton.[3] The AOM consists of an anti-reflection coated Tellurium Dioxide *(TeO_2)* crystal with a piezo-electric transducer glued onto one end. The central frequency of the acoustic wave is $\omega_c / 2\pi = 200MHz$. The acoustic wave creates a transient transmission grating which diffracts the optical wave. at the Bragg angle. The acoustic velocity v_s in the crystal is 4.2km/s and the light pulse spends less than 10ps in the crystal, so the acoustic wave moves less than 0.002 $\lambda_{acoustic}$ during the transit of the light field through the crystal. Since the acoustic wave is essentially frozen as the optical pulse travels through the crystal, the complex amplitude of the acoustic wave traveling through the crystal in the y direction, $A(t)\cos\omega_c t = A(y/v_s)\cos\omega_c t$, is mapped onto the optical field $E(\omega)$ as it passes through the AOM. If some of the dispersed optical field encounters a weak acoustic wave, that frequency is attenuated; if the acoustic wave carrier is shifted by a phase angle ϕ, that phase shift is imposed on the optical field. Our pulse shaper has a total efficiency of about 10%, including the diffraction efficiency of the AOM and the diffraction efficiency of the gratings. We use the diffracted light and we discard the undiffracted "zero order" beam. This allows full modulation of both amplitude and phase in the shaped beam. The shaped beam then has the form

$$E_{shaped}(\omega) = E_{input}(\omega) \times a(\omega) \times e^{i\phi(\omega)t} \tag{1}$$

where $a(\omega)e^{i\phi(\omega)} = A[y(\omega)/v_s]$.

The damage threshold of the AOM is approximately $4J/cm^2$. The pulse shaper follows the first stage regenerative amplifier, and it precedes the final amplifier, in order to limit the input pulse energy to $100\mu J$. The shaped pulses are amplified further in an unsaturated multipass final amplifier. The resolution of an AOM-based shaper can be quoted in terms of "effective pixels". Our shaper was designed to have about 200 effective pixels over its complete length. However, we are currently using a shorter modulator, limiting our number of pixels to 170.

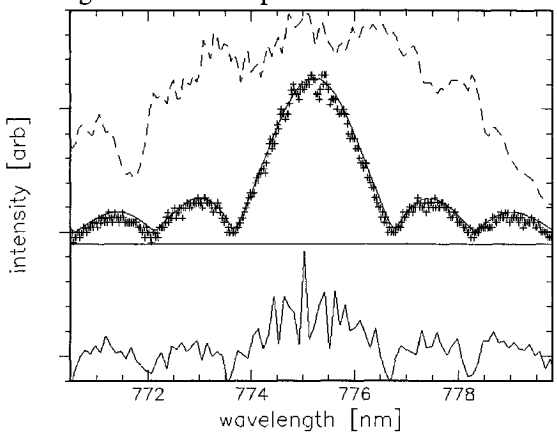

Figure 1. Sinc shaped spectrum with the model spectrum, unshaped spectrum and array sent to the waveform generator boards. The top curve is the unshaped spectrum. Below it is the measured spectrum with the overlaid solid curve showing the model spectrum. The bottom curve shows the array sent to the waveform generator for the measured spectrum.

The shaped pulses are measured using spectral interferometry. In this technique, the shaped laser pulse is merged with an unshaped reference pulse on a beam splitter, and then the combined pulses are analyzed in a spectrometer. The signal is a spectrally resolved interference. If the reference pulse is known to have flat spectral phase, then the amplitude beating of the output beam is a direct measure of the spectral phase function.

ATOMIC WAVE PACKETS

Sculpting technique

Rydberg atoms are a testing ground for quantum classical correspondence, and for quantum state preparation and measurement.[4] We can use Rydberg atoms to explore ideas in strong field quantum control and quantum information problems. This section describes our development of wave packet "sculpting" and the quantum interference techniques used to view these sculptures.[5].

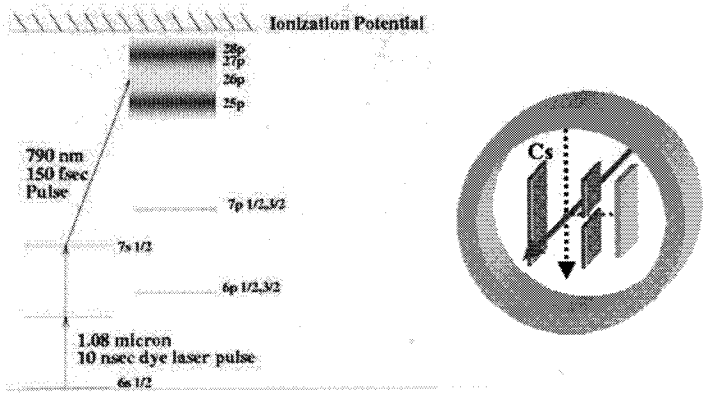

Figure 2. Excitation scheme for producing sculpted Rydberg wave packets in atomic Cs. Right: schematic of the interactions region, showing the intersection of the atomic beam and the laser beams. Field ionization plates and a charged particle detector are also shown.

The creation and measurement of our Rydberg wave packets occurs inside a vacuum chamber, where and effusive beam of Cs atoms intersect one or more laser beams (see Figure 2). Ground state atoms are excited to the 7s state using a two-photon transition at 1.08 μm, produced by Raman shifting the output of a pulsed dye laser. Sculpted laser pulses then excite the atoms to Rydberg states. This produces coherent superpositions of $p_{1/2}$ and $p_{3/2}$ states with principal quantum number between 24 and 35. In most applications we are only interested in tracking the shape over the first few picoseconds. The natural time scale for the spin-orbit interaction that splits the $p_{1/2}$ and $p_{3/2}$ states is much longer than this (on the order of 100 *ps* for the states considered here) so the wave packet is described quite well without electron spin, in the *nlm* basis. In that case, only l=1 states are excited. The value of the magnetic quantum number m then depends on the relative orientation of the quantization axis and the laser polarization that induces transitions from the *7s* state. In most cases they are perpendicular, so we excite equal amplitudes of $m = \pm 1$ states.

The shape of a wave packet $\Psi(\mathbf{x},t)$ is determined by the amplitude and phase of the constituent eigenstates:

$$\Psi(\mathbf{x},t) = \sum_{np} a_n e^{i\Phi_n} u_{npm}(\mathbf{x}) e^{-i\omega_n t} \tag{2}$$

In the limit of weak excitation, the complex amplitude is simply given by Fermi's Golden Rule, so it is proportional to the dipole matrix element times the resonant electric field:

$$a_n e^{i\Phi_n} \propto E(\omega_{np} - \omega_{7s})\langle npm|z|7s\rangle \propto E(\omega_{np} - \omega_{7s})/n^3 \tag{3}$$

The quantum state amplitude and phase are therefore directly related to the amplitude and phase of the sculpted optical field.

Amplitude Measurement

The quantum state amplitudes are measured using state-selective field ionization[6]. A uniform electric field is slowly applied to the Rydberg system to induce field ionization. The field produces a saddle point in the coulomb potential. A hydrogenic Rydberg state with m=0 and binding energy E ionizes rapidly when the saddle point in the potential reaches the value $F=(4/9)E^2$ in atomic units ($2000V/cm \times [20/n^4]$).

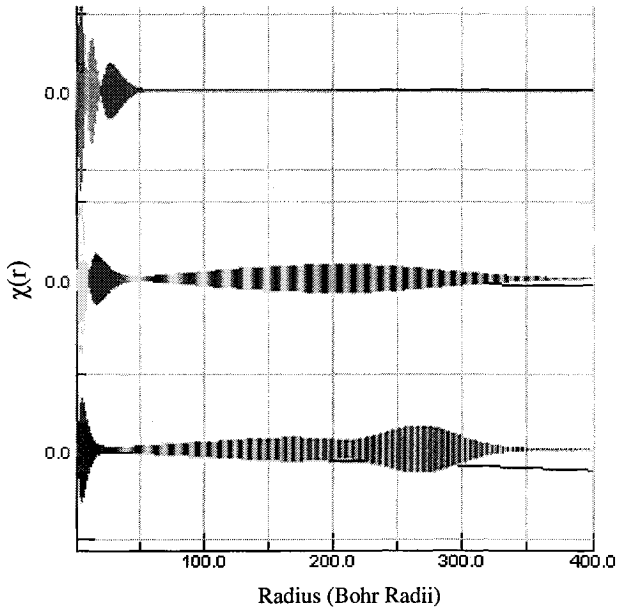

Figure 3. Calculation of a simple p-state radial wave packet undergoing field ionization. The different shades of gray represent the quantum phase of the wave packet. Top: Bound state wave packet consisting of the 2p, 3p, and 4p states of hydrogen with equal amplitude. Middle: Above the critical field for ionizing 4p, the wave packet splits into an ionized portion on the right, and a bound wave packet consisting of the 2p and 3p states. Bottom: For a larger field, only the 2p state remains bound.

The field must increase slowly compared to the characteristic dynamical time scale for the Rydberg state, which is the corresponding Kepler orbital period, $2\pi n^3$. The situation is similar for higher m and for atoms with a non-hydrogenic ion core: the critical ionization field is proportional to E^{-2}.

When a wave packet is subjected to the slow ramp, it does not necessarily ionize the moment that one of its n-states reaches the critical electric field. Instead, the ionization occurs with probability proportional to the square of the amplitude for that state. An ensemble of identical states will ionize with a distribution of critical fields that maps the squares of the individual state amplitudes, as shown in the calculation in figure 3, and the data in figure 4.

Ramped field measurements only reveal the amplitude of the states that make up a wave packet. The shape of the quantum sculpture also depends on the relative phase of these states, which can only be discovered through an interference measurement.

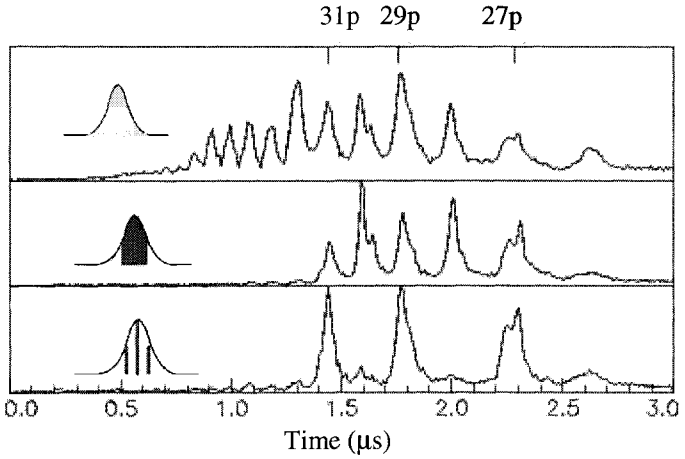

Figure 4. Ramped field ionization signal for three different sculpted wave packets in cesium. The insets show the amplitude function of the shaped light pulse that made these wave packets.

Phase Measurement

The relative phases of the quantum states evolve according to $e^{i\Delta\omega t}$, so any phase measurement must reference a particular laboratory time. We measure the phase using a holographic technique similar to spectral interferometry mentioned in the first section of this paper. The measurement proceeds by exciting the atoms with a second, *reference* wave packet with a time delay τ with respect to the sculpted packet. The reference excitation has all of its orbitals relatively real:

$$\Psi_{ref}(\mathbf{x},t) = e^{i\omega_{gs}t}\sum_{np} b_n u_{npm}(\mathbf{x}) e^{-i\omega_n t} \tag{4}$$

The optical field that excites such a wave packet is a transform-limited pulse arriving at time τ. The probability for state i following the excitation is

$$P_i = |a_i|^2 + |b_i|^2 + 2|a_i||b_i|\cos[(\omega_i - \omega_{gs})\tau - \phi_i] \tag{5}$$

In principle, ϕ_i can be extracted from this directly. In practice, though, the laser system is not stable with respect to frequencies on the scale of ω_i-ω_{gs}, which is an optical frequency. Instead, then, the phases are extracted by constructing a correlation function

$$r_{ij} = \frac{\langle P_i P_j \rangle - \langle P_i \rangle \langle P_j \rangle}{(\Delta P_i)(\Delta P_j)} = \cos[(\omega_i - \omega_j) - (\phi_i - \phi_j)] \tag{6}$$

where (ΔP_i) is the root-mean-squared value of P_i averaged over many laser pulses.

An example of a wave packet sculpture reconstructed in this way is shown in figure 5.

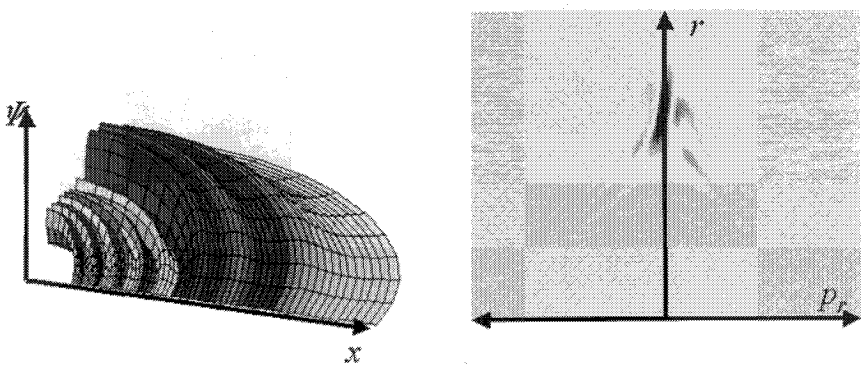

Figure 5. Two views of a sculpted wave packet. Left: Schrodinger wave function. The amplitude is shown as a function of x and z for a *p*-state wave packet oriented along x. Gray scale represents phase. Right: Wigner representation of the same wave packet in the (r,p_r) phase space plane. Here, gray scale represents amplitude.

QUANTUM INFORMATION APPLICATIONS

Quantum wave packets can also be used to store, retrieve, and manipulate information. This has been discussed recently in connection with the prospect of solving very large or difficult problems with a "quantum computer." While a Rydberg atom may be far too small to solve large problems, it contains the basic elements necessary for quantum computation. These are long coherence times, a large state space, and the entanglement of several degrees of freedom.

Consider, for example, the storage of a simple binary number, such as 000001000. A wave packet could encode this number in various ways. For example, one could load an *n*-state quantum wave packet with an *n*-bit number according to the prescription that at a specified time *t*, the phase is real and positive for binary 0, but real and negative for binary 1. Since every state in the wave packet has equal amplitude, ordinary spectroscopic techniques such as state-selective field ionization cannot reveal which state stores the binary 1. This bit is hidden from view. If the same data were stored in a classical binary register with *n* locations, one would have to search each location to find the marked bit. The search would take, on average, *n*/2 steps; however, the rules of quantum state manipulation provide some simple methods for revealing the marked bit.

If the quantum data register is formed by excitation from the atomic ground state in the weak field limit, then one may take advantage of the probability amplitude that remains in the ground state to find the marked bit by quantum holography. Figure 6 describes the method. A search, or "decoder" wave packet is prepared by exciting the atom with a simple pulse where all of the quantum phases are real and negative. This is, in fact, the very same "reference" pulse that was used to measure the phases in the sculpted wave in the previous section. In this case, the superposition results in destructive interference of any states where a binary 0 was stored, but constructive addition to any states with a binary 1. The combined wave packet then has the same

information as before, but now it is encoded into quantum amplitudes rather than phases. These can then be read out easily using state-selective field ionization.[7]

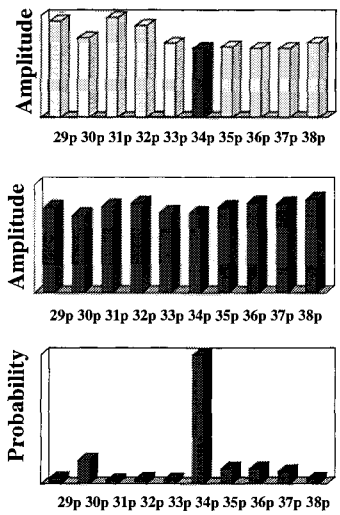

Figure 6. (a) Bar graph representing a Rydberg data register for the binary number 0000010000. The binary bit is encoded into the phase of the n-state, so that binary 0 states are real and positive, while binary 1 states are real and negative. (b) The decoding wave packet has equal amplitudes, and all negative real phases. (c) The superposition of (a) and (b) amplifies the binary 1 bits, while destructive interference destroys the binary 0 bits.

This is a simple example of a general class of search algorithms that make use of the properties of superposition and quantum interference, introduced by L.K. Grover.[8] Our particular implementation of a Grover-style search algorithm has some unresolved difficulties if the register is too large. The simple form of the decoding pulse only works in the perturbation theory limit, where almost all of the probability amplitude in the wave packet resides in the "launching" state (7*s* for our work in Cs.) If there are too many states in the Rydberg wave packet, the launch state will become depleted. The data retrieval is still possible, but now the unitary transformation that amplifies the "1" bits and suppresses the "0" bits must depend on the total pulse energy, and possible other factors. In other words, we move into *the strong field regime.*

The connection between strong field dynamics and quantum information processing seems inescapable. To study this in Rydberg systems, we need to have methods to transfer large amounts of probability amplitude between Rydberg states. We have begun to study this with half cycle pulses of broadband terahertz radiation, which may be able to redistribute population, and amplify marked states in Rydberg systems.

LEARNING ALGORITHMS

Feedback and Learning Control

The techniques described in the previous sections are "feed-forward," since the construction and measurement processes make no use make no use of the measured results. The "feedback" loop is closed by the experimenters themselves, who may adjust the pulse shaper in response to information gathered by wave packet holography. This particular type of feedback is more properly called "learning," since the readjustment of the apparatus does not occur during a measurement, but rather follows the data acquisition, so that corrections can be made to future experiments.[9] We have implemented an automated form of learning control on wave packets in Rydberg states, and have found that an arbitrary wave packet can be made to converge on a "target" sculpture shape in only one or two iterations.[10]

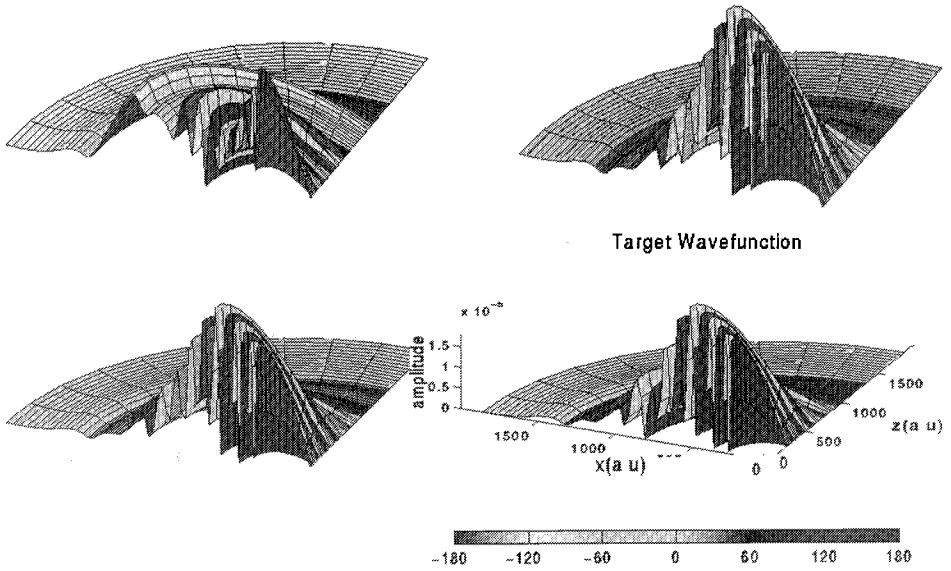

Figure 7. Learning feedback control of a Rydberg wave packet. The desired target wave packet is shown on the lower right. The initial guess produced by the pulse shaper is on the upper left. After two iterations, shown on the upper right and lower left, the experiment converges to the target shape.

The amplitude and relative phase of each eigenstates in the wave packet was determined by quantum holography and state-selective field ionization. Then, the system computer calculated the difference between each of these amplitudes and phases, and those of the desired target state. These phase and amplitude differences were then added to the phase and amplitude of each corresponding excitation wavelength in the Bragg modulator. This simple linear feedback algorithm is effective for two reasons: First, the system requires full access to the reconstruction information. The Rydberg system accomplishes this via quantum state holography.

Second, there must be a simple relationship function connecting the error signals and the correction information. This second requirement is particularly easy for the Bragg modulator, where each eigenstates uses a different wavelength, which traverses a different part of the device. In fact, convergence is very rapid, at least in principle, since the correction phase is the precise phase change for the corresponding excitation wavelength. A second iteration is only needed because of imprecise knowledge of the Bragg modulator response function. Nonlinearities in the Bragg detector response and other technical control problems are automatically corrected in the feedback loop.

One important consequence of automatic learning control is that the system is capable of adapting to changing initial conditions and maintaining a fixed output (the target wave function) with a changing input. We have demonstrated this by subjecting the pulse shaper to pulse shape changes or additional delays. The learning feedback control has no difficulty maintaining the target wave function, so long as the time delay between the shaped wave packet and the reference pulse is short enough to guarantee coherence

Genetic Search Algorithms for Learning Control

The linear feedback described in the preceding section is only effective for systems with a known Hamiltonian and eigenstates spectrum, and for laser interactions in the weak-field limit. The more general situation is more complicated, but also more useful. Nonlinear optical interactions are used to generate new coherent light sources, and also to probe dynamics. In principle, a strong driving field could be shaped to enhance the desired nonlinear interaction, so that pulse shaping could become a general tool for nonlinear dynamics. One obstacle is that the Hamiltonian for any complex molecular system is not known well enough, and with out it one cannot predict likely excitation pathways or derive the optimal pulse shapes. Learning algorithms may offer a solution to these problems. In this approach, the experiment runs itself by means of an intelligent feedback loop. It tries various pulse shapes, assesses their success in achieving the desired target excitation, and uses the knowledge gained in this way to improve the pulse shapes on subsequent experiments, all without the intervention of the researcher.

In its simplest form, learning control simply optimizes the pulse shape by controlling dispersion in the laser amplifier and the nonlinear medium, or by filtering the spectrum. The more general problem of pulse shaping is more daunting: Consider that the pulse shaper can control the amplitude and phase of well over 100 different frequency components with 8 bits of resolution (i.e. 256 different amplitudes) per frequency component. Therefore there are over 256^{100} different pulse shapes to try. Furthermore, each frequency component is not necessarily independent of the phase and amplitude of the others, so they cannot each be optimized independently. Additional requirements are that the algorithm be robust in the face of experimental noise and be capable of escaping local maxima in an enormous and rough potential energy landscape.

We have been studying learning control in several different nonlinear systems, using a search strategy known as the genetic algorithm (GA).[11] "Genetic" in this case means that the algorithm creates new pulses through a non-local approach based on

splicing together traits of successful "parent" laser pulses, rather than by following a fitness gradient function, as in other evolutionary methods

In our GA implementation, each individual corresponds to a pulse shape, which is encoded as a string of floating point numbers (the individual genome) specifying the phase and amplitude at the various frequency components of the laser pulse. In the first generation, the population consists of sixty individual pulse shapes, chosen at random. We have studied quantum dynamics where the target measurement depended on the shape of the driving laser field. The experiment is performed for each pulse shape in turn, and the results assigned a numerical fitness value based on the result. This fitness value determines the chances that a particular pulse shape is selected to reproduce. For example, "roulette wheel" selection, an individual's reproduction probability is proportional to its fitness.

Adaptive Operators

Reproduction involves modifying and combining elements of previous individuals to create new individuals. Operators that act on the genomes of the pulse shapes carry this out. Operators that we use include *multi-point crossover, mutation, averaging, creep, smoothing, choice of genome basis, and polynomial phase mutation.*
Here is a brief description of how the different operators work:

- *Crossover* exchanges one or more sections of the genome from each of two or more parents. The resulting two gene strings are the two new children pulse shapes.
- *Mutation* randomly alters individual genes in the genome.
- *Averaging* produces children by averaging the gene values of two or more parents.
- *Creep* is mutation where the final gene value is constrained to fall close to the parent value.
- *Smoothing* averages nearby gene values in the genome.
- *Choice of basis* changes the basis vectors of the genetic code. For example, the genome representing frequency and phase might be replaced with its inverse Fourier transform genome, where the pulse shape is recorded as amplitude vs. time.
- *Polynomial-phase mutation* produces children by replacing a portion of a gene string with a polynomial fit.

A well-chosen set of operators can greatly enhance the performance of the GA and lend additional physical insight. But the proper choice is usually far from obvious, so we allow the algorithm to adapt itself by letting it choose how often to use a given operator to produce new children. The use of adaptive operators helps speed up convergence, and, perhaps more importantly, it helps shed light on the control mechanism at work. The reproductive operators compete to produce new pulse shapes. In other words, better operators produce more offspring.

A lower bound ensures that every operator always has some chance of being used during reproduction, a necessity if the operator is ever going to be able to increase its fitness. Some operators also involve an internal parameter, such as the mutation rate.

For example, we have found that the algorithm's performance is improved if two-point crossover operator has a large initial weighting. Crossover is more effective in the beginning of the algorithm when there is maximal genetic diversity, since it does a good job of mixing up the gene strings between parents. It becomes less effective as the GA converges to the best solutions, since at this point there is much less genetic diversity in the population, so there is not longer a need to drastically change the gene strings.

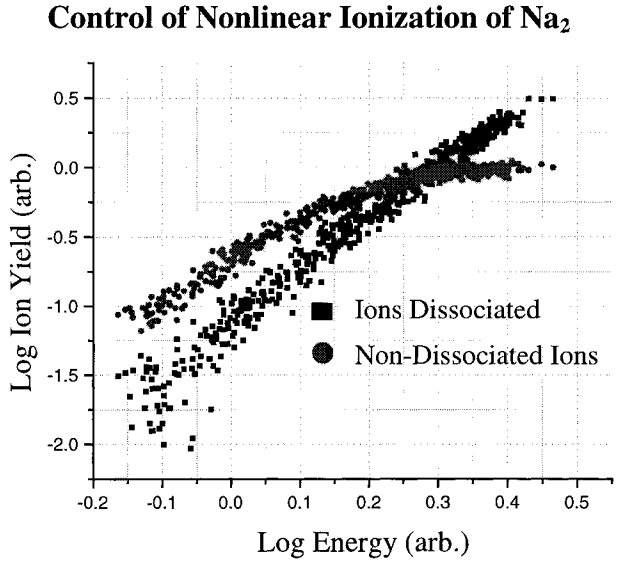

Figure 8. Ion yield vs. intensity for multiphoton ionization of Na_2.

The photoionization of diatomic sodium with 790 *nm* radiation provides an interesting test of the adaptive GA. There are two different final states for this process, which are reached by different nonlinear absorption pathways: *dissociative ionization* ($Na_2 + 5\gamma \rightarrow Na + Na^+ + e^-$) and *non-dissociative ionization* ($Na_2 + 4\gamma \rightarrow Na_2^+ + e^-$). A simple fitness function may be constructed from the ratio of $[Na^+]/[Na_2^+]$ observed in the reaction chamber, which in our case is a supersonic molecular beam with an ion mass spectrometer. Conventional wisdom of high order perturbation theory predicts that the lower order non-dissociative process dominates at low intensities, but that the higher order dissociative rate increases faster as the intensity of the laser pulse increases. We also expect this could be modified by intermediate states, which could Stark shift into or out of lower order resonance with intensity. Indeed, a simple intensity vs. yield curve bears this out, and shows clearly how the non-dissociative process deviates as we enter the strong field regime (figure 8), in a way that favors the dissociative process even more strongly.

Recent work on resonant photoabsorption in atoms has shown that the *shape* of the laser pulse can also exert a strong influence on the absorption cross section.[12] This is because the shape of the pulse can alter the *nonlinear spectrum* (i.e. the Fourier transform of $E^n(t)$, even though it cannot change the *linear spectrum* (F.T. of $E(t)$).[13]

Could this effect also help to optimize the yield control over ionization of molecular sodium? We asked the GA to find out. Figure 9 shows the results for two different solutions, optimizing either the dissociative or non-dissociative yields.

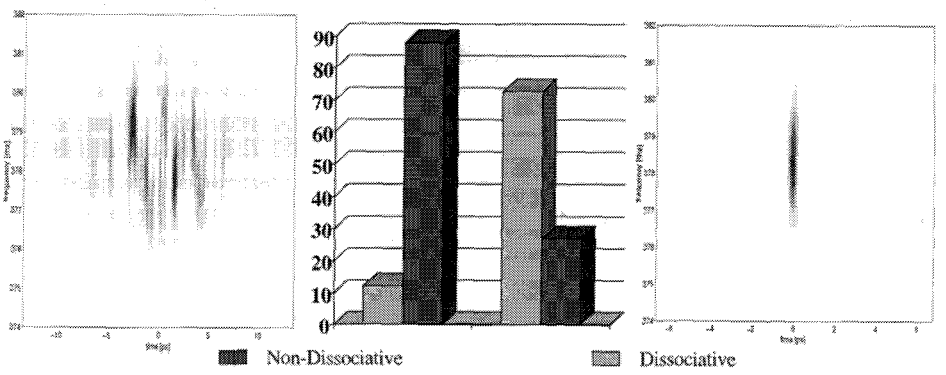

Figure 9. Optical spectrograms and yields for two solutions to multiphoton ionization of Na_2. The spectrograms give a qualitative picture of the pulse shapes, which show the laser intensity vs. time (horizontal) and frequency (vertical). Nondissociative ionization (spectrogram on the left) is favored when the pulse energy is spread over as long a time as possible, while dissociative ionization (spectrogram on the right) is favored when the light is concentrated into a very short time.

We found that pulse length, rather than pulse symmetry was the dominant mechanism for control in this case.

Selective Excitation of Quantum Modes in Molecular Liquids

Our most successful use of the GA in quantum systems thus far has been in selective excitation of C-H and C-D stretch modes in organic molecules in liquid phase.[14] Control has been demonstrated in methanol, benzene, and in mixtures of regular and deuterated benzene (C_6D_6). Liquids pose a special challenge to strong field physics, because of rapid relaxation, and also because many nonlinear processes influence the light and make it difficult to define an observable that is related to the desired fitness.

The results of control experiments in methanol illustrate some of the features of the control search algorithms. The laser pulses in these experiments were intense enough to produce self phase modulation in the $1cm$ path length through the liquid. Stimulated Raman scattering into the C-H stretch modes created additional spectral structure on the output pulse. The Stokes shifts for the asymmetric and symmetric modes are 2942 cm^{-1} and 2847 cm^{-1} respectively, which therefore place them far outside the laser bandwidth, but within the white light continuum generated by self phase modulation. By Fourier's theorem the laser pulse duration is therefore long compared to the vibrational period of either stretch mode. In this non-impulsive regime, selective Raman modes cannot be seeded directly with the laser light. Nonetheless, we found that the GA could teach the laser to excite the symmetric and

asymmetric stretch modes either together or individually by changing the shape of the driving pulse.

The fitness criterion was the integrated spectral intensity of stimulated Raman scattering into one or more Stokes peaks, which indicates excitation of the desired vibrational modes. Figure 10 shows evidence for selective excitation of the symmetric and asymmetric C-H stretch modes excited by pulse shapes found by the algorithm.

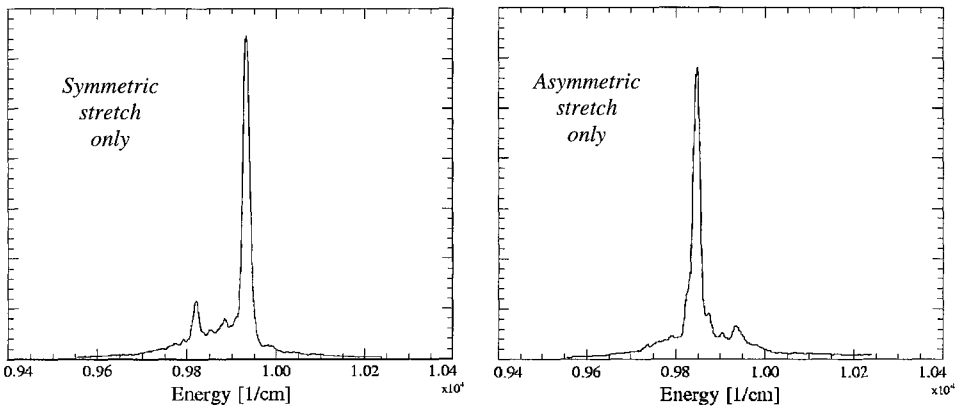

Figure 10. Selective Stokes peaks in the forward scattered light with a methanol sample. The driving laser pulse had a central frequency of 12,700 cm^{-1}

Further insight into the selective excitation mechanism can be gained through examination of the shaped pulses that effected the control. Figure 11 shows the time and frequency map of the electromagnetic field pulses optimized by the GA for exciting the two C-H stretch modes in methanol.

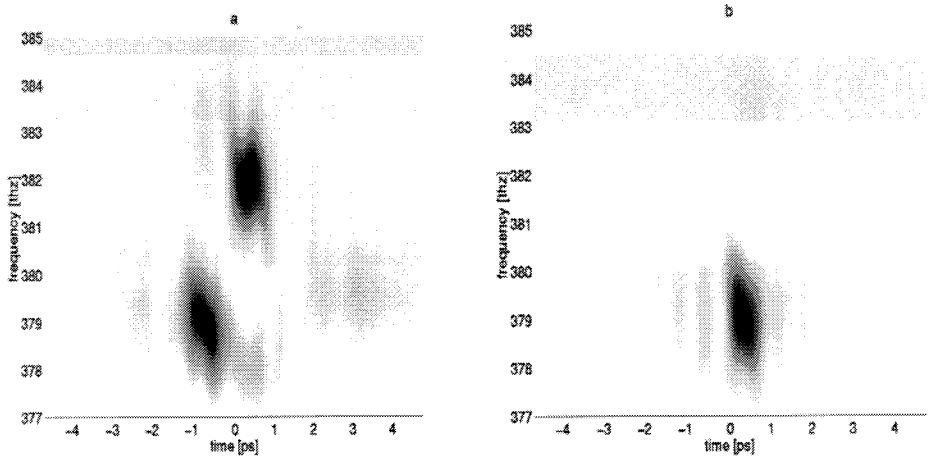

Figure 11. Spectral power distributions for shaped pulses optimized for driving the symmetric (on the left) and asymmetric (on the right) stretch modes in methanol.

ACKNOWLEDGMENTS

The experiments described in this paper were carried out by graduate students Thomas Weinacht, Jaewook Ahn, and Brett Pearson, and undergraduate student James White. We gratefully acknowledge support from the National Science Foundation, grant 9414335, and the Army Research Office.

REFERENCES

1 C. Spielman, P. F. Curley, T. Brabec, and F. Krausz, IEEE J. Quant Electron. QE-30 1100 (1994), and references therein.
2 D Strickland and G Mourou.. Opt. Commun., **55,** 447 (1985).
3 J. X. Tull, M. A. Dugan and W. S. Warren, Adv. Opt. Mag. Resonance 20, 1 (1990); A. M. Weiner D. E. Leird J. S. Patel, and J. R. Wullert , J. of Quantum Electronics **28** (1992).
4 T. Gallagher, Rydberg Atoms. Cambridge, Massachusetts: Cambridge Press, 1995.
5 T.C. Weinacht, J. Ahn, and P.H. Bucksbaum, Phys. Rev. Letters **80**, 5508 (1998).
6 T. Gallagher, *op. cit* 4.
7 J. Ahn, T.C. Weinacht, and P.H. Bucksbaum, Science, **287**, 463 (2000)
8 L.K. Grover, Phys. Rev. Lett. **79**, 325 (1997); Phys. Rev. Lett. **79**, 4709 (1997).
9 H. Rabitz and R. Judson, Phys. Rev. Lett. **68**, 1500 (1992).
10 T.C. Weinacht, J. Ahn, P.H. Bucksbaum, Nature **397**, 233 (1999).
11 Genetic algorithm: Davis, L. Ed. *Handbook of Genetic Algorithms*, Van Norstrand Reinhold: New York, (1991).
12 D. Meshulach, Y. Silberberg, Nature **398,** 298 (1998).
13 P.H. Bucksbaum, Nature **396**, 217 (1998)
14 T.C. Weinacht, J.L. White, P.H. Bucksbaum, Jour. of Phys. Chem. A, **103**, 10166 (1999).